

Noise Considerations for TEMPEST Data

Peter Wolfram*

*Xcalibur Multiphysics
10 Compass Road
Jandakot, Perth
Western Australia
peter.wolfram@xcaliburmp.com*

Teo Hage

*Xcalibur Multiphysics
10 Compass Road
Jandakot, Perth
Western Australia
teo.hage@xcaliburmp.com*

Eric Steele

*Xcalibur Multiphysics
10 Compass Road
Jandakot, Perth
Western Australia
eric.steele@xcaliburmp.com*

SUMMARY

The noise characteristic of an AEM system is crucial not only for designing the signal processing strategy but more importantly for interpreting the data in terms of an earth model. Ad hoc estimates of noise are often all that is available to the user of an AEM data set, leaving noise as the “elephant in the room”. We present a rigorous approach to estimating noise from first principles. We illustrate how such estimates may be obtained from high-altitude calibration data and then be applied to processing and interpretation of TEMPEST data.

Key words: TEMPEST, Noise Model, Data Processing Conductivity Inversion.

INTRODUCTION

Noise estimates are no longer just “error bars” for display in pretty pictures, but they are being used in algorithms that further process the survey data either using weighted least squares solutions to systems of equations or iterative solutions of linear systems during conductivity inversion.

Noise estimates for conductivity inversions can be too generous which means large “error bars” and the possibility that the fitting model is not well determined. Jones’ (2019) proposal to minimise the cross-correlation between the fitting residuals alleviates this problem to some extent, but better noise estimates are preferable. Conversely, when error estimates are too tight, then the usual Chi-squared criterion will not achieve convergence because the fitting error will always be larger than the data error.

We have constructed a noise model for TEMPEST data from first principles and illustrated its features with examples. Narrow-band noise such as VLF and the spectral gaps resulting from the finite transmitter switching time are automatically down-weighted when the inverse standard deviation or variance are used as weights in signal processing algorithms. The noise estimates are also being used for improved conductivity depth transformation (CDT) and we tested them for improved layered earth inversion (LEI).

METHOD AND RESULTS

A Noise Model for TEMPEST

Using upper-case letters to indicate Fourier Transforms, the voltage measured in each receiver coil is:

$$V_r = -\frac{\mu_0 A_r A_t}{4\pi} R_{rf} R_c j\omega \{g + R_g\} I \quad (1)$$

where A_r is the effective coil area, A_t is the transmitter loop area*turns, R_{rf} is the frequency response of the combined anti-alias filter and digitizer, R_c is the frequency response of the induction coil, g is the geometric coupling factor between the transmitter loop and the receiver coil, R_g is the frequency response of the ground, I is the transmitter current, and $j = \sqrt{-1}$, and $\omega = 2\pi f$ with f being the frequency. Similarly, the voltage recorded from the transmitter monitoring device is

$$V_t = R_{tf} R_{tc} I \quad (2)$$

where R_{tc} is the calibration factor of the current monitor device, R_{tf} is the frequency response of the anti-alias filter and digitiser, and I is the current. The transfer function T from the transmitter to the receiver is then

$$T = \frac{V_r}{V_t} = -\frac{\mu_0 A_r A_t}{4\pi} \frac{R_{rf}}{R_{tf} R_{tc}} R_c j\omega \{g + R_g\} \quad (3)$$

The transfer function T_a for the high-altitude calibration run is the same but without the R_g ground response term. By forming the ratio T/T_a the quantity Ψ is obtained which constitutes the deconvolution of the system transfer function from the measured transfer function and was first published by Lane et al (2000):

$$\Psi(\omega, \mathbf{r}) := \frac{T(\omega, \mathbf{r})}{T_a(\omega)} = \frac{g(\mathbf{r})}{g_a} + \frac{R_g(\omega, \mathbf{r})}{g_a} \quad (4)$$

The independent variables are included explicitly to highlight the dependence on location \mathbf{r} and frequency ω . The data example in Figure 1 shows increased noise at the high frequency end of the spectrum.

Rasmussen et al (2017) investigate the effect of noise in TEM signals (ground and airborne) on the deconvolution. Their noise model consists of *external noise* (stationary and nonstationary components, e.g., from radio signals, spherics, and motion-induced noise, or nonlinear effects such as amplifier saturation due to a strong primary-field component in the on time), and *internal noise* (stationary components only, e.g., thermal noise, electronics noise from oscillators and power supplies, and quantization noise in the ADC). Their noise terms are complex functions of frequency and could in principle include bias spectra that have not been accounted for elsewhere. In particular, the noise model of Rasmussen et al (2017) does not allow for coupling variations between transmitter and receiver (g and g_a would be 1), it does not treat the deconvolution of high-altitude spectra from survey altitude spectra, and it also does not explicitly allow for an airframe response.

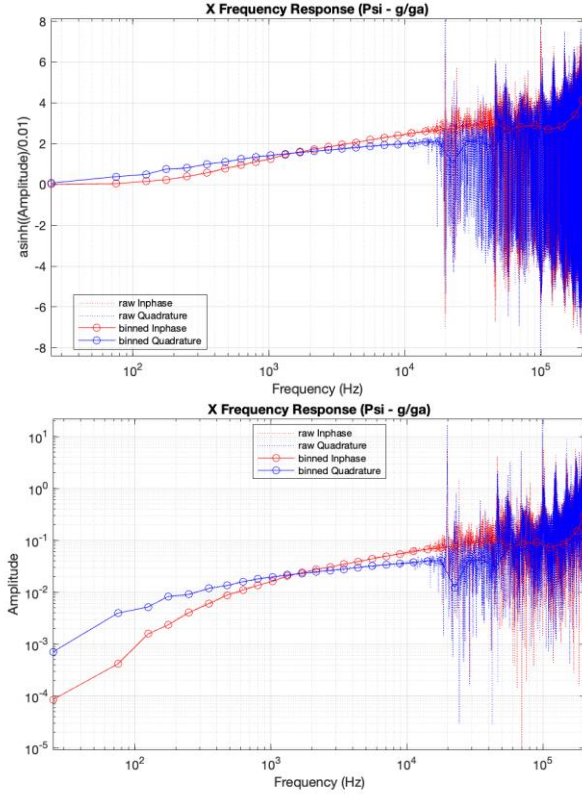


Figure 1: A snapshot of the frequency response at one location along a flightline showing the noise character with asinh scaling (upper panel) and with logarithmic scaling (lower panel). Dotted lines are the raw frequency response, the circles are weighted averages for logarithmically spaced frequency bins. The logarithmic scaling shows the transmitter nulls and VLF lines in the high frequencies more clearly but it hides the fact that the noise can go negative. The data are from a TEMPEST test flight with 25 Hz base frequency and 400 kHz acquisition rate.

All these noise features may be accounted for by including in equations 1 and 2 two extra terms representing complex spectra, one for the external noise $N_{ext}(\omega)$ (which is modified by the receiver parameters) and one for the internal noise $N_{int}(\omega)$. The receiver spectrum contains both whereas the transmitter spectrum contains only the internal kind (noted simply as N_i). Equations 1 and 2 then become

$$V_r = -\frac{\mu_0}{4\pi} A_t A_r R_{rf} R_{cl} \omega I (g + R_g + N_{ext}) + N_{int} \quad (5)$$

$$V_t = R_{tf} R_{tc} I + N_t$$

Forming the transfer functions T and T_a and then the frequency response Ψ is achieved with the help of Taylor expansion and neglecting second order terms. The main assumption for simplifying the final expression is that the noise does not change between the reference altitude and the survey altitude. Combining various noise terms into a single variable N_{mod} results in an expression for the *measured* Ψ_m equivalent to equation 4:

$$\Psi_m(\omega, \mathbf{r}) = \Psi(\omega, \mathbf{r}) + N_{mod}(\omega)(1 - \Psi(\omega, \mathbf{r})) + N_{add}(\omega) \quad (6)$$

where $N_{mod}(\omega)$ stands for the sum of internal and external complex noise spectra that have been modulated by coupling variations, and we have introduced $N_{add}(\omega)$ to allow for a complex bias and additive noise in Ψ_m . The ground response R_g

is zero along any of the high-altitude lines resulting in an equation that may be used for determining the noise terms:

$$\Psi_m(\omega, \mathbf{r}_a) = \frac{g(\mathbf{r}_a)}{g_a} + N_{mod}(\omega) \left(1 - \frac{g(\mathbf{r}_a)}{g_a}\right) + N_{add}(\omega) \quad (7)$$

The complex term $N_{add}(\omega)$ can be estimated from the high-altitude *reference line*. This line is flown “straight and level” which minimizes any variations of the coupling ratio $g(\mathbf{r})/g_a$ so the round bracket is close to zero and the *modulated* noise term becomes negligible. The complex bias and standard deviation may then be estimated using the entire reference line:

$$N_{bias}(\omega) \approx \text{mean}_{\{\mathbf{r}=\mathbf{r}_{ref}\}} \left(\Psi_m(\omega, \mathbf{r}) - \frac{g(\mathbf{r})}{g_a} \right)$$

$$N_{std}(\omega) \approx \text{stddev}_{\{\mathbf{r}=\mathbf{r}_{ref}\}} \left(\Psi_m(\omega, \mathbf{r}) - \frac{g(\mathbf{r})}{g_a} \right) \quad (8)$$

Figure 2 illustrates the resulting noise spectra for a reference line flown with the standard TEMPEST system.

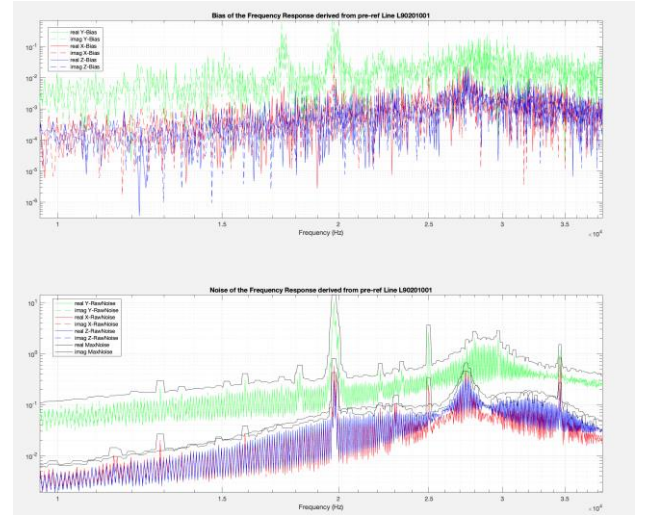


Figure 2: A high-altitude reference line showing the high frequency region of the complex bias of the Frequency Response (upper panel, solid lines for inphase, dashed for quadrature) and real-valued standard deviation (lower panel). The x,y,z components are red, green, blue respectively, and the black curves in the middle panel are the moving maximum over a sliding window with user-defined width. The Y component has higher noise because it is nearly null-coupled with the transmitter.

Figure 3 shows the windowed Bfield obtained from the high-altitude reference line. This is the result of processing the frequency response Ψ_m as if the line was a survey line. Although the noise estimates discussed here are for the frequency domain, the processed reference line may be used to derive noise estimates for the Bfield windows.

The modulated noise may be estimated from the high-altitude *swoop line*. The average is restricted to only those samples with strong geometrical coupling variations so that the denominator is different enough from zero.

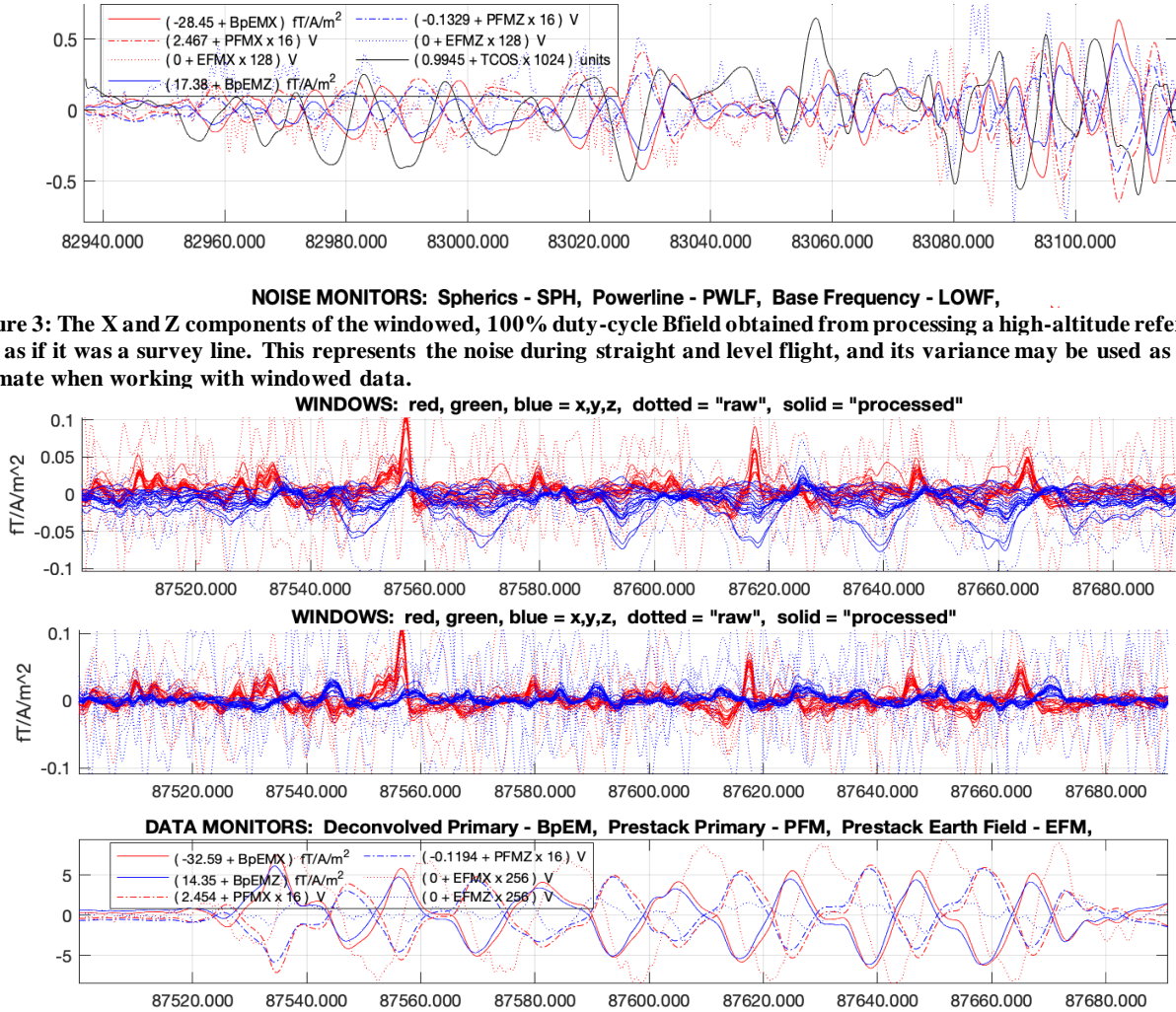
$$N_{mod}(\omega) = \text{mean}_{\{\mathbf{r}=\mathbf{r}_{swoop}\}} \left(\frac{\Psi_m(\omega, \mathbf{r}) - N_{bias}(\omega) - \frac{g(\mathbf{r})}{g_a}}{1 - \frac{g(\mathbf{r})}{g_a}} \right) \quad (9)$$

This is not strictly “noise” because it includes any response from the metallic airframe that is sensed when the geometrical

coupling between transmitter and receiver changes. A correction for this effect is applied during processing of the survey lines as follows

$$\Psi(\omega, \mathbf{r}) = \frac{\Psi_m(\omega, \mathbf{r}) - N_{bias}(\omega) - N_{mod}(\omega)}{1 - N_{mod}(\omega)} \quad (10)$$

Figure 4 illustrates the windowed Bfield processed along the swoop line without and with removing the airframe response, indicating that the effect of the airframe is typically small and below the overall noise level.



Weighted Least Squares Solvers in Frequency Domain

Weighted least squares solvers may be employed to find the solutions to a linear system of equations (LSE): $\mathbf{A}^* \mathbf{x} = \mathbf{B}$, where \mathbf{B} is the data vector (the frequency response), \mathbf{x} is the unknown vector and \mathbf{A} is the LSE matrix. The weighted least squares solution minimizes

$$(\mathbf{B} - \mathbf{A}^* \mathbf{x})^T \mathbf{W} (\mathbf{B} - \mathbf{A}^* \mathbf{x})$$

where the covariance matrix \mathbf{W} may be constructed with the inverse of the standard deviation $N_{std}(\omega)$ from Equation 8 or the inverse of the variance on the diagonal.

We have established and solved such systems of equations for

- reducing the high-frequency noise in the frequency response (where \mathbf{A} contains smoothness constraints and \mathbf{x}

is the smoothed data vector) before further processing, and for

- inverting the raw or binned frequency response data directly from the frequency domain to an earth conductivity model (where \mathbf{A} contains constraints and regularization and \mathbf{x} is the model vector).

Figure 5 shows the effect of fitting a piecewise cubic polynomial to the high (> 15 kHz) frequencies using weighted least squares. The high-frequency noise is successfully rejected.

Figure 6 illustrates how a wide (0.5 decades) weighted convolution filter has a stronger smoothing effect than the narrow (0.1 decades) binning shown by circles in Figures 1 and 5. It successfully extends the frequency response through the noisy high-frequency region.

Both examples result in a very similar windowed Bfield because the windowing further rejects high-frequency noise except in the very first few windows (not shown here).

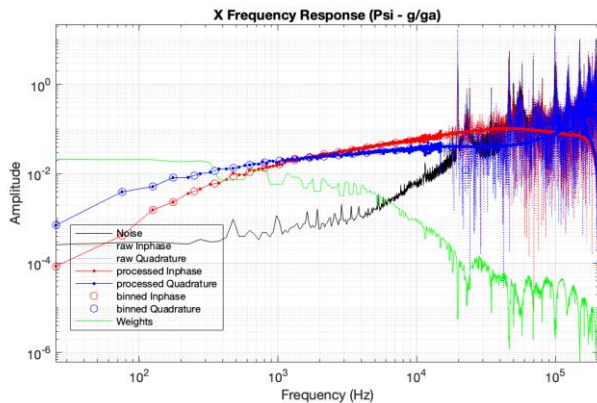


Figure 5: Same data as Figure 1 but including noise (black curve), weights (green), and processed data (red and blue with dot symbols) that were replaced by a weighted least squares fit above 15 kHz. The circles are the same as before: bins with a width of 0.1 decades.

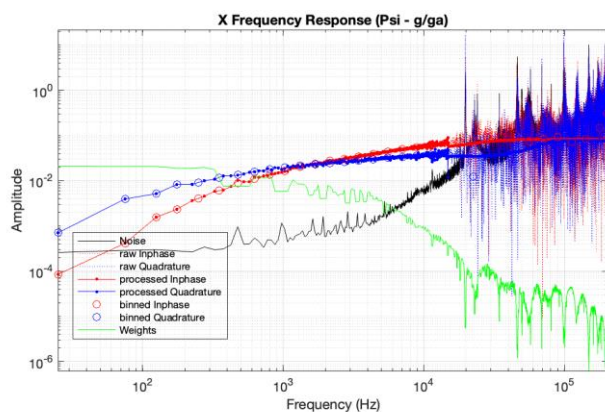


Figure 6: Same data as Figure 1 but including noise (black curve), weights (green), and processed data (red and blue with dot symbols) that were filtered above 15 kHz with a 0.5 decades width Hanning filter combined with data weights.

In order to calculate a Conductivity Depth Transform (CDT), the raw or binned frequency response is first fitted with a sum of complex basis functions using weighted least squares that also include constraints for stabilising the solution. Each basis function is the Fourier transform of an exponential decay. The resulting coefficients are then used to construct the step response which is in turn matched with the field of a receding image of the transmitter resulting in a conductivity versus depth function (Wolfgram and Karlik, 1995). The result compared well with conductivity sections generated in other ways.

As proof of concept only, we have also implemented and successfully tested a Layered Earth Inversion (LEI) that uses the raw or binned frequency response (dotted lines or circles in Figures 1, 5 and 6) together with the noise estimates as input.

Noise Estimates for Windowed Data in Time Domain

In the same manner as the noise and bias spectra were derived from the frequency response along high-altitude calibration lines, time-domain noise and bias may be derived from the final windowed Bfield calculated along these same lines (Figure 3). We have done this in order to derive quality control data (Figure 6) but the noise may also be converted to weights for further data processing or conductivity inversion in time domain.

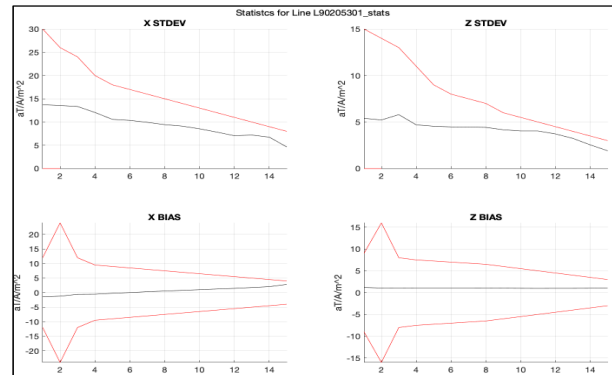


Figure 7: Statistics (black curves) for a high-altitude reference line. The red curves show noise bounds for quality control. The Window numbers are along the horizontal axis and atto-Teslas per Am^2 on the vertical axis.

CONCLUSIONS

We have captured the noise characteristic of TEMPEST data as complex noise and bias estimates for the raw frequency response and showed how this may be exploited for processing and interpretation. Data weights derived from the noise estimates effectively depress the major noise sources of VLF and transmitter spectral gaps when used in processing and inversion algorithms. Tests with CDT and LEI produced clean conductivity sections from the raw frequency response.

ACKNOWLEDGMENTS

New processing algorithms had become necessary to replace historic processing code that was no longer adequate for recent TEMPEST developments. None of this work would have been possible without the help and the patience of those in Xcalibur in Jandakot who are dealing with ‘real’ data on a daily basis.

REFERENCES

- Jones, A.G., 2019, Beyond chi-squared: Additional measures of the closeness of a model to data. AEGC 2019, Perth, Extended Abstracts.
- Lane, R., A. Green, C. Golding, M. Owers, P. Pik, C. Plunkett, D. Sattel, B. Thorn, 2000, An example of 3D conductivity mapping using the TEMPEST airborne electromagnetic system. *Exploration Geophysics* 31, 162-172.
- Rasmussen, S., N.S. Nyboe, S. Mai, J.J. Larsen, 2017, Noise properties of Fourier deconvolution for time-domain electromagnetic soundings. *Geophysics* 82 (5), E257-E266.
- Wolfgram, P., G. Karlik, 1995, Conductivity-depth transform of GEOTEM data. *Exploration Geophysics* 26, 179-185.